CrossMark

RESEARCH ARTICLE

Examining the effect of Zn dopant on physical properties of nanostructured SnS thin film by using electrodeposition

Farhad Niknia[1] · Farid Jamali-Sheini[2] · Ramin Yousefi[3]

Abstract Undoped and Zn-doped SnS nanostructures have been successfully synthesized through an electrodeposition process by using $SnCl_2$ and $Na_2S_2O_3$ as precursors on fluorine-doped tin oxide-coated (FTO) glass substrates with different zinc concentrations. The structure, surface morphology, and the optical properties of the synthesized films are studied. The X-ray diffraction patterns of the SnS nanostructure confirm the orthorhombic structure. Scanning electron microscopy shows thin films with homogeneous and uniform surface as well, by adding Zn ions, morphology of SnS films changed from cubic to rod. Energy dispersive spectroscopy shows presence of Zn in the films. All samples are characterized by UV–Vis reflectance measurement in the wavelength range 500–1200 nm. The energy band gap values, calculated from optical measurement of reflectance, are between 1.46 and 1.49 eV, being suitable for absorbers layers in the photovoltaic applications. Eventually, studying the photocurrent responses of the nanostructures revealed that the Zn-doped SnS nanostructures exhibited better response than the undoped SnS nanostructures.

✉ Farid Jamali-Sheini
faridjamali2003@yahoo.com; faridjamali@iau.ahvaz.ac.ir

[1] Department of Materials Science and Engineering, Islamic Azad University, Ahvaz Branch, Ahvaz, Iran

[2] Department of Physics, Islamic Azad University, Ahvaz Branch, Ahvaz, Iran

[3] Department of Physics, Islamic Azad University (I.A.U), Masjed-Soleiman Branch, Masjed-Soleiman, Iran

Graphical Abstract
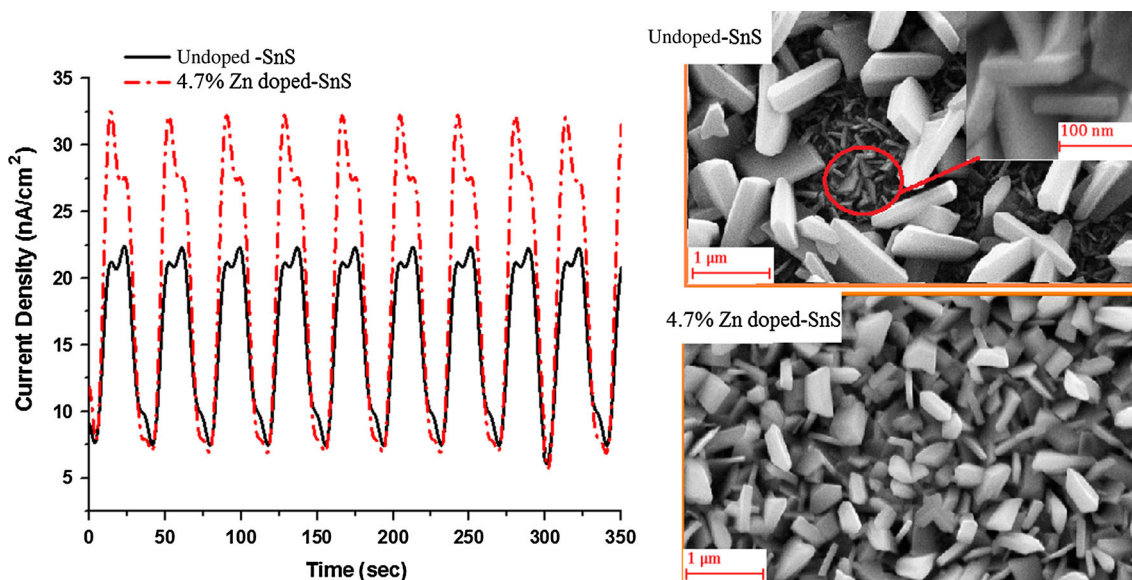
1 Introduction

As part of a thrust in environmentally aware materials research, new inorganic light absorber materials are sought to be inexpensive, environmental-friendly, and it helps to improve solar cell energy conversion efficiencies [1, 2]. These absorber materials can be used to build photovoltaic devices with the standard type of thin-film heterojunction configuration, or even be used in novel nanostructured configurations, such as three-dimensional (3D) solar cell [3] or extremely thin absorber (ETA) solar cells [4–7].

Tin monosulfide is a promising semiconductor, as it absorbs light within peak solar radiation wavelengths (885–1200 nm) [8–11]. It has a high absorption coefficient ($\alpha > 10^4$ cm^{-1}) [8–10]. However, few researches have been performed on this material as on similar metal monosulfides, such as CdS. The most commonly synthesized phase for photovoltaic materials research, the orthorhombic α-SnS (herzenbergite), is p type, which is characterized by a direct optical transition of $\sim$1.3 eV [8–11]. The addition of an impurity to the SnS compound has a special effect on structural, optical, and electronic properties of SnS semiconductor. For instance, Niknia et al. prepared Pb-doped SnS thin films by using an electrodeposition technique to improve optical properties. They found a red shift for the band gap values from 1.46 to 1.40 eV with an increase in the Pb concentration [12]. Seal et al. deposited Sb- and In-doped SnS thin films. Films composed of primarily orthorhombic SnS were electrodeposited on titanium substrates. It had a smaller effect on the measured photocurrent, and at higher precursor concentration (>5 %) the dopants resulted in the formation of secondary phases of Sb and In oxides with reduction in the measured photocurrent [13]. For the Ge- and Sb-doped SnS films subjected to anneal at 200–350 °C in N$_2$, the band gaps of 200 °C-annealed films remained unchanged, while those of 300- and 350 °C-annealed films decreased with the annealing temperature because of the evaporation of Ge and Sb, respectively. Hsu et al. obtained this result by using solvothermal route [14]. Recently, Patel et al. have carried out doped SnS by pulsed DC magnetron sputtering of elemental Cu at different temperatures. An improvement in the photocurrent density from 1.1 to 1.8 mA/cm^2 was observed in the photo-electrochemical cell by this doping process [15]. Kumar et al. reported Ag-doped SnS thin films were deposited onto microscopic glass substrates at a substrate temperature of 350 °C by the spray pyrolysis technique. The lower electrical resistivity of 8.63×10^{-1} Ω cm and the optical band gap of 1.33 eV were obtained at 8 % of Ag [16]. Kiruthigaa et al. prepared Ce-doped SnS$_2$ thin films using a solid state reaction at low temperature and solvent-free. Optical investigation revealed that the energy band gap value of Ce-doped SnS$_2$ decreased compared to that of undoped [17]. Moreover, SnS thin films were deposited at different potentials by Mariappan et al. [18]. They managed to produce smooth and uniform films that were suitable for photovoltaic application. The modified chemical vapor deposition (CVD) process was used for deposition of Sb-doped SnS thin film. Small amounts of antimony ($\sim$1 %) were found

to greatly increase the electrical resistance of the SnS. Higher concentrations ($\sim$5 %) of antimony had not converted the SnS: Sb to low-resistivity *n* type conductivity [19]. There are very few reports on the Zn-doped SnS thin films prepared by hydrothermal which have demonstrated low values for their carrier concentration and conductivity [20]. To date, no research has targeted method the Zn-doped SnS thin films by the electrodeposition method; therefore, this study aimed to investigate the effect of Zn dopant on SnS thin films by using the electrodeposition technique and photocurrent properties.

2 Experimental section

2.1 Synthesis of SnS and Zn-doped SnS nanostructures

The synthesis of SnS thin films was performed in a conventional three-electrode electrochemical cell. Aqueous solutions of $SnCl_2$ and $Na_2S_2O_3$ at the concentrations of $\sim$2 × 10^{-3} M (100 ml) and 20 × 10^{-3} M (100 ml) were prepared in different beakers. All solutions were transferred to a beaker and by adding a few drops of H_2SO_4 the pH of the solution was adjusted to 1.5. Form the literature survey, it is known that when the pH is equal to, or smaller than 2.5, atomic ratio of Sn/S is less than 1; when the pH is equal to, or larger than 3.0, Sn/S is greater than 1. The Sn/S ratio increases by increasing the pH value, because the supply of S by reaction (1) is diminished when the pH is raised [21].

$$S_2O_3^{2-} + 6H^+ + 4e^- \leftrightarrow 2S + 3H_2O \tag{1}$$
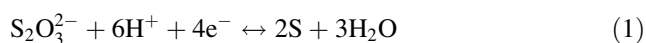
The reaction scheme for the formation of the SnS on a cathodic surface is represented by two equations as follows:

$$Sn_2O_3^{2-} + 2H_{aq}^+ \rightarrow S_{(s)} + SO_{2(g)} + H_2O_{(l)} \tag{2}$$

$$Sn_{aq}^{2+} + S_{(s)} + 2e^- \rightarrow SnS_{(s)} \tag{3}$$
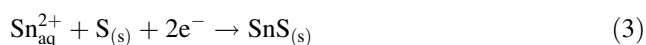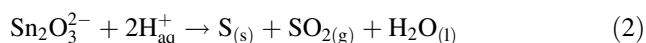
The first equation is representing the well-known decomposition of thiosulfate in acid solution giving rise to elemental S and SO_2. The decomposition of thiosulfate in acid solution is a classic example of a disproportionation reaction which is a specific type of redox reaction in that the same species is simultaneously reduced and oxidized to form two different products. In our case, the two S ions of starting thiosulfate having a (2+) chemical state give rise, as products of the disproportionation reaction, to one atom of elemental S, having zero as chemical state, and one S ion of the sulfurous acid having a (4+) chemical

state, thus perfectly balancing the electron exchange between the S species. Although the second reaction does not clearly indicate, which species is reduced to allow SnS precipitation, it is supposed that the reduction of Sn^{2+} is favorable at the cathode to form Sn(s) and then SnS(s) formation on the surface [22, 23]. This is because of the fact that it is the continuation of the electrical current. In fact, this would be the case since 'S' is not necessary for the continuation equation. Moreover, based on the enthalpies of formation of SnS and ZnS (−108 and −206 kJ/mol respectively) it is expected that the ZnS is formed on the surface of the cathode; however, because of the following reasons, the dominate phase is SnS: (1) electromotive force for the reduction half of Sn^{2+} is more than Zn^{2+}, (2) the concentration of Sn^{2+} is higher than Zn^{2+}. On the other hand, the probability of the formation of ZnO in a low pH is very low; therefore, this is reasonable that the main product on the surface of cathode should be SnS or Zn-doped SnS that all of characterization results confirm this claim. The thickness of the SnS film was determined to be about 1 μm by the weight difference method assuming that the sample is uniform and dense as that of the bulk having a density of 7.4 g cm^{-3}.

The temperature of the solution was kept at 80 °C. An FTO-coated glass substrate, platinum sheet, and saturated calomel electrode (SCE, $E0$ = 0.244 V vs. NHE) served as the working, counter, and reference electrodes, respectively. The electrodes were ultrasonically cleaned in acetone and methanol successively for 10 min. A computer-controlled electrochemical analyzer (potentiostat, Autolab, A3ut71167, The Netherlands) was used to maintain the cathodic polarization condition at −1.2 V with respect to the SCE. The deposition period was 45 min. In order to make the electrolyte for doping, an aqueous solution of $ZnCl_2$ at a concentration of $\sim$2 × 10^{-3} M was prepared in a separate beaker. By adding different quantities of this solution (1 cc, 3 cc, or 7 cc) to different beakers, separate experiments were carried out. The specimens were called Zn 0, Zn 1, Zn 2, and Zn 3 for the undoped and doped specimens with different amounts of the solution, respectively. After conducting each experiment, the deposited SnS thin film was washed softly in pure water, and naturally dried in the air. The SnS films were uniform and their color was dark brown. All the used chemicals were analytical grade reagents and water used was double-distilled water. At least three specimens were synthesized under identical experimental conditions and characterized by various analytical techniques in order to check the reproducibility and repeatability of the results.

2.2 Materials characterization

The structure of the deposited films was characterized by a Philips X'Pert Pro MPD X-ray diffraction (XRD) system with a Cu Kα radiation source. The surface morphology and composition of the films were analyzed by an FESEM, Ziess ΣIGMA VP field emission scanning electron microscope (FESEM) with an energy dispersive X-ray (EDX) analysis attachment, which works at an operating voltage of 20 kV. The optical properties were investigated using the photoluminescence (PL) and UV–Visible (UV–Vis) spectra recorded at room temperature. The UV–Vis diffuse reflectance spectra (DRS) were recorded using a UV–Visible spectrophotometer (Perkin Elmer-Lambda 950) over a wavelength range of 500–1200 nm. The PL was measured with a photoluminescence spectrometer (Varian-Cary Eclipse) using a xenon lamp as the light source with an excitation wavelength of ∼440 nm.

Solar cell devices were assembled using the deposited films as working electrodes and Pt foil as counter electrodes, which were sealed in as sandwich cell that was filled with the electrolyte in a 100-μm-thick spacer. The electrolyte liquid was Γ/I_3^-. The photocurrent response was measured by a potentiostat (Autolab, A3ut71167, The Netherlands) using a 100-W xenon lamp as the light source. The incident light intensity was calibrated by a standard solar cell. The illuminated area of the specimens was 0.5 cm^2, and the distance between the working electrode and the lamp was 30 cm. The photocurrent was recorded continuously during the ON and OFF periods of the lamp. All the experiments were carried out under ambient conditions.

3 Results and discussion

3.1 Morphological and microstructural analysis

3.1.1 X-ray diffraction

The XRD patterns of the SnS film (undoped and doped) deposited onto the FTO glass substrate are shown in Fig. 1. All the deposited films are polycrystalline. These patterns consist of the same peak centered at approximately $2\theta = 37.807°$, which correspond to the (1 1 4)-reflection of the SnS lattice with an orthorhombic structure. When the amount of ZnCl$_2$ in the deposition solution increased, the diffuse dispersion peaks of XRD patterns increased as well. The patterns exhibit several XRD peaks corresponding to the different planes based on JCPDS card nos. 079-2193, 01-075-0925, and 032-1361. It indicates that all the diffraction peaks of the deposited SnS films are coincident with the corresponding diffraction peaks of orthorhombic
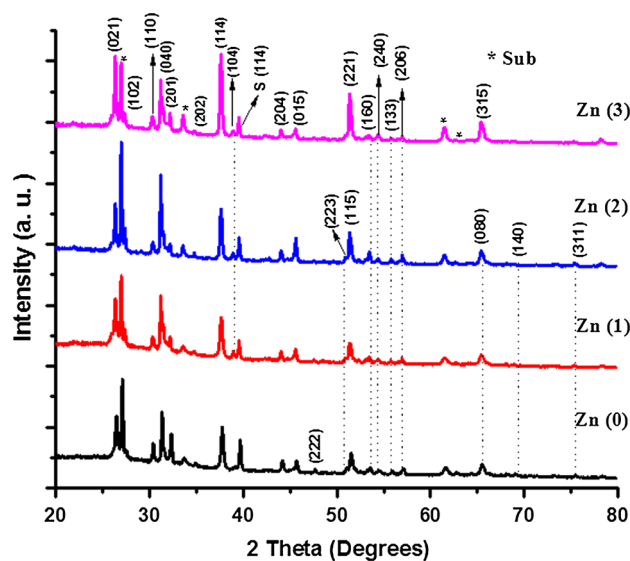
Fig. 1 XRD patterns of undoped and Zn-doped SnS thin films grown on FTO glass substrates

SnS. The lattice parameters were calculated using the observed values of $2\theta = 37.80°$ for the (1 1 4) plane and the d values (inter-planar spacing) for the orthorhombic structure, which is given by

$$\frac{1}{d^2} = \frac{h^2}{a^2} + \frac{k^2}{b^2} + \frac{l^2}{c^2} \tag{4}$$

where (h k l) are the Miller indices of the plane concerned and a, b, and c are the lattice parameters. The values of the lattice parameters of the SnS film were calculated to be $a = 0.433$ nm, $b = 1.1248$ nm, and $c = 0.399$ nm with $a/c = 1.085$, which were in good agreement with the standard values of the lattice parameters taken from the JCPDS card file data. The strongest peak at 26.45° indicates that the SnS films are preferentially oriented along the (0 2 1) plane. Preferential orientation of SnS films is due to the fact that the growth process is controlled by nucleation [24]. Therefore, the films are SnS with orthorhombic structure. In addition, the crystalline size was evaluated using the Scherer formula. The average crystallite sizes of the SnS films were calculated to be 47.6 nm (Zn (0)), 62.5 nm (Zn (1) and Zn (2)), and 51.3 nm (Zn (3)). For lower Zn concentration, the crystallite size increased and decreased for a higher concentration. The decreased intensity of the XRD peaks for the higher concentration showed a reduction in the crystallinity due to the incorporation of more Zn atoms into the SnS lattice. Moreover, the increase of the ZnCl$_2$ content causes the broadening of the SnS (1 1 4) peak and the decreasing of other small peaks. When the amount of ZnCl$_2$ in the deposition solution increases, the diffuse dispersion peaks of XRD patterns also increase. It is clear that the crystalline properties

of the thin film depend on doping concentration impurity: it causes the broadening of peaks, particularly (1 1 4) orthorhombic peak. Zainal [25], observed similar behavior for SnS thin films from aqueous solution.

### 3.1.2 Scanning electron microscope and energy dispersive analysis

Figure 2 shows FESEM micrographs of (a) Zn (0), (b) Zn (1), (c) Zn (2), and (d) Zn (3). The Zn0 specimens demonstrated well-defined crystallographic facets in different ranges, one of which was in the form of sheets with a thickness of 20–50 nm and the other was in the form of a cubic rod smaller than 1 μm. By adding Zn ions, the surface of the specimen became rod structures (Fig. 2b). With increasing the Zn concentration, the surface of the specimens changed to regulated structures. Moreover, it was also observed that the surface of the films, which were grown at lower and higher concentrations, exhibited deeper holes between the grains. These differences between the shape and density of the specimens can be explained by the presence of Zn ions in the electrolyte. The grain sizes are between 47.6 and 62.5 nm. It should be noted that the grain sizes estimated from the XRD pattern are generally smaller than those obtained by SEM determination since the estimation from Eq. (4) is generally the sub grain size on the

principle of X-ray diffraction, while the grain observed by SEM should be the result of sub-grain collection [26]. The composition of the films was determined by the EDX analysis which indicated that the atomic ratios of Zn 1, Zn 2, and Zn 3 were 1.2, 3.1, and 4.7, respectively, and that there was no evidence of the oxygen signal (Fig. 3). Zn 0 showed the presence of only Sn and S.
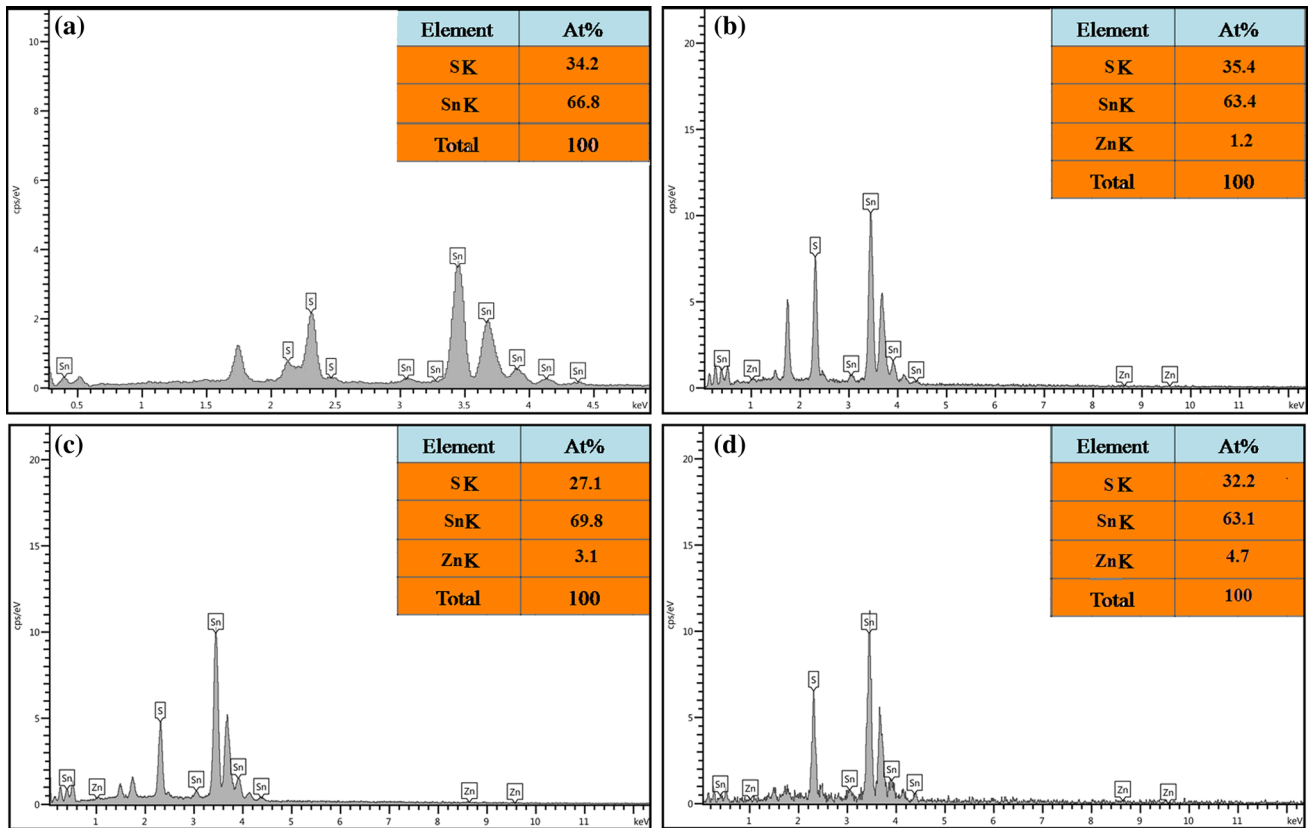
3.2 Optical properties

3.2.1 Photoluminescence

Figure 4a and b illustrate the PL emission spectra of the undoped and Zn-doped SnS nanostructures, respectively. The SnS nanostructures show two strong emission bands centered at 470 nm (blue emission) and 530 nm (green emission). Figure 4b depicts the band-to-band emission (∼829 nm) of the SnS nanostructures, which is in accord with the energy band gap of 1.46 eV. The strong blue-green emission might be similar to that of SnS nanoparticles, which is ascribed to the influence of a large quantity of defects [27–30]. During the preparation process, a high density of sulfur and tin vacancies may be expected. Besides sulfur and tin vacancies, various kinds of defects, such as interstitials, stacking faults, have also been introduced in the nanostructures [27]. In addition, comparing
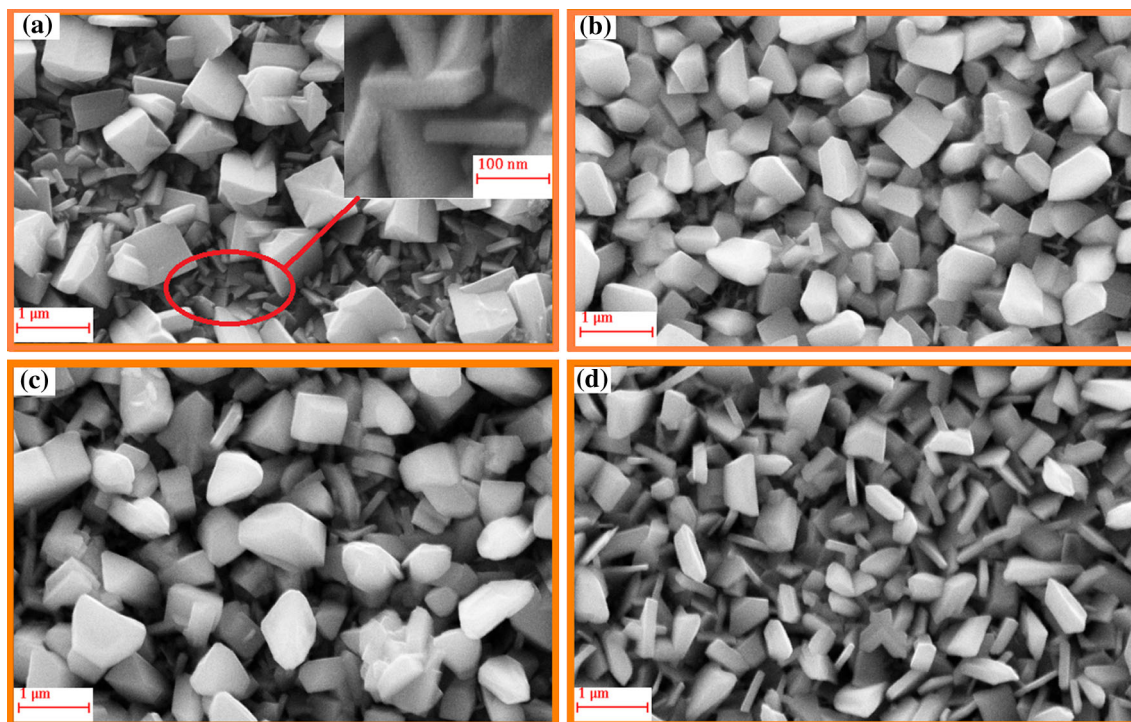
Fig. 2 SEM micrographs of synthesized Zn-SnS thin films grown on FTO glass substrates for **a** Zn (0) (undoped), **b** Zn (1), **c** Zn (2), **d** Zn (3)

Element	At%
S K	34.2
Sn K	66.8
Total	100

Element	At%
S K	35.4
Sn K	63.4
Zn K	1.2
Total	100

Element	At%
S K	27.1
Sn K	69.8
Zn K	3.1
Total	100

Element	At%
S K	32.2
Sn K	63.1
Zn K	4.7
Total	100

Fig. 3 EDX analysis of synthesized Zn-SnS thin films grown on FTO glass substrates for **a** Zn (0) (undoped), **b** Zn (1), **c** Zn (2), **d** Zn (3)
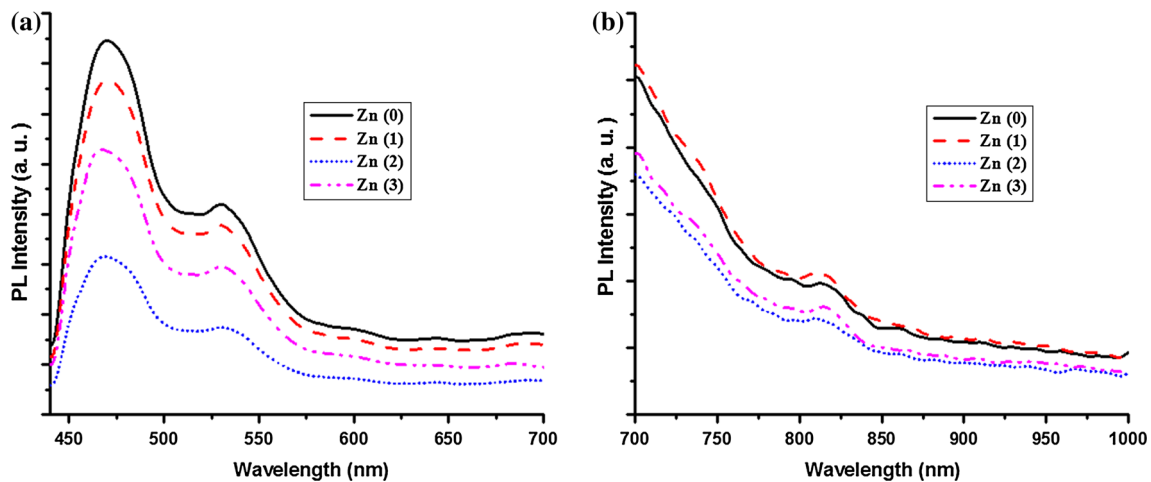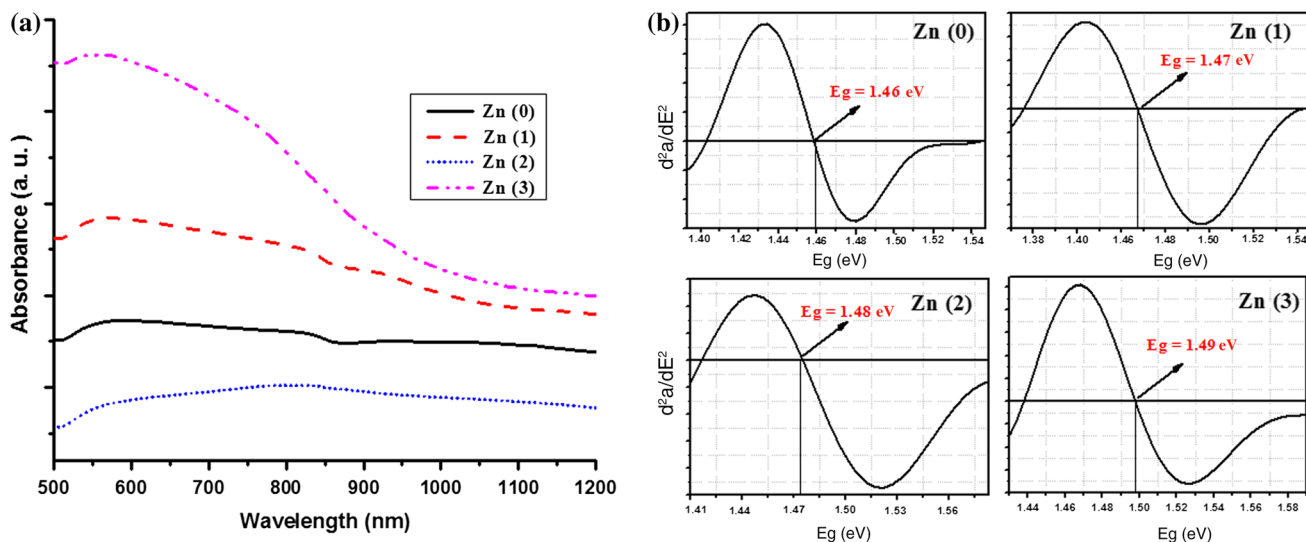

Fig. 4 a and **b** PL spectra of the undoped and Zn-doped nanostructured SnS thin films

with the undoped SnS, the PL spectra of the nanostructured Zn-doped SnS thin films showed an obvious blue shift in the emission. This blue shift can be attributed to the large difference between the energy band gap values of SnS (~ 1.5 eV) and ZnS (3.54 eV). The strong blue-green emission also suggests that the SnS thin films have potential application to blue and green light emitters or any other optical devices.

3.2.2 UV–Vis reflectance

The optical absorbance spectra of electrodeposited SnS thin films that were recorded as a function of wavelength in the range 500–1200 nm are shown in Fig. 5a. The spectra revealed a characteristic absorption peak of SnS for the specimens made with different concentrations of Zn and the undoped SnS, which can be attributed to the electron
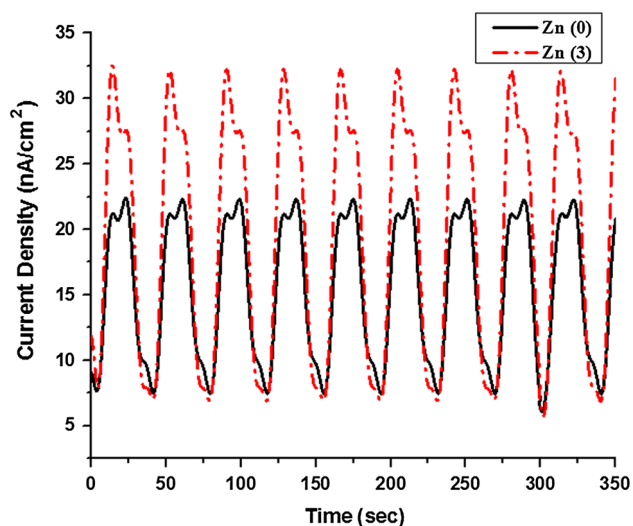
(a)

Fig. 5 **a** UV–Visible absorption spectra of the undoped and nanostructured Zn-doped SnS thin films, **b** derivative of the UV–Vis absorption spectra of the undoped and nanostructured Zn-doped SnS thin films

transitions from the valence band to the conduction band. In addition, the direct band gap can be estimated from the maximum of the first derivative of the absorbance plot versus energy also from intersection of the second derivative with energy axle [31-34] as shown in Fig. 5b. The figure shows band gaps of 1.46, 1.47, 1.48, and 1.49 eV for the undoped, Zn (1), Zn (2), and Zn (3) specimens, respectively.

3.2.3 Photovoltaic characterization

Figure 6 shows the photocurrents of the specimens under pulse illumination light. Under illumination, the

Fig. 6 The typical photocurrent response of the undoped and nanostructured Zn-doped SnS thin films under pulse illumination of the xenon light

photocurrent of the films quickly increased and remained relatively constant during the illumination. The photocurrent response of the film had a sharp-edge peak when the light was out. Generally, electrons and holes are generated after light absorption with energy equal to, or greater than the band gap of the semiconductor. Some kinds of doped transition metals such as Zn can provide more negative charge carriers and/or shallow trap levels for photo-generated electron and hole so as to inhibit the recombination and enhancing charge-generation efficiency [35–37]. The photocurrent response of Zn-doped SnS is higher than the SnS.

4 Conclusions

The undoped and Zn-doped SnS nanostructures were obtained using electrodeposition technique on FTO substrates. The XRD analyses indicated that the films were polycrystalline in nature and that they exhibited an orthorhombic crystal structure. Because of the Zn doping, the crystallite size increased from 47.6 to 62.5 nm. SEM studies showed that the SnS films represented most homogeneous surface and that the morphologies of the films changed less with variation of Zn concentration. In addition, the EDX results showed the presence of Sn, Zn, and S elements in the doped films. Optical measurements revealed an increase in the band gap, which was attributed to the effect of incorporating the Zn ions into the SnS lattice. In addition, the results showed that the Zn ions played important roles in enhancing the photocurrent and improving the sensitivity of the synthesized films. This

indicated that the properties of nanostructured SnS films can be altered by Zn doping, which could be used in optoelectronic applications.

References

1. Memming R (1980) Solar energy conversion by photoelectro-chemical processes. Electrochim Acta 25:77–88
2. Mathews NR, García CC, Torres IZ (2013) Effect of annealing on structural, optical and electrical properties of pulse electrode-posited tin sulfide films. Mater Sci Semicond Process 16(1):29–37
3. Ernst K, Belaidi A, Konenkamp R (2003) Solar cell with extremely thin absorber on highly structured substrate. Semicond Sci Technol 18:475–479
4. Ernst K, Engelhardt R, Ellmer K, Kelch C, Muffler HJ, Lux-Steiner MC, Könenkamp R (2001) Contacts to a solar cell with extremely thin CdTe absorber. Thin Solid Films 387(1–2):26–28
5. Clément CL, Zaera RT, Ryan MA, Katty A, Hodes G (2005) CdSe-Sensitized p- CuSCN/Nanowire n-ZnO Heterojunctions. Adv Mater 17(12):1512–1515
6. Zaera RT, Ryan MA, Katty A, Hodes G, Bastide S, Clément CL (2006) Fabrication and characterization of ZnO nanowires/CdSe/CuSCN eta-solar cell. Chim C R 9(56):717–729
7. Larramona G, Choné C, Jacob A, Sakakura D, Delatouche B, Péré D, Bayón R (2006) Nanostructured photovoltaic cell of the type titanium dioxide, cadmium sulfide thin coating, and copper thiocyanate showing high quantum efficiency. Chem Mater 18(6):1688–1696
8. Reddy NK, Reddy KTR (2005) SnS films for photovoltaic applications: physical investigations on sprayed Sn_xS_y films. Phys B 368:25–31
9. Reddy NK, Reddy KTR (2006) Optical behaviour of sprayed tin sulphide thin films. Mater Res Bull 41(2):414–422
10. Devika M, Reddy NK, Ramesh K, Ganesan R, Gunasekhar KR, Gopal ESR, Reddy KR (2007) Thickness effect on the physical properties of evaporated SnS films. Electrochem Soc 154(2):H67–H73
11. Nair MTS, Nair PK (1991) Simplified chemical deposition technique for good quality SnS thin films. Semicond Sci Technol 6:132–134
12. Niknia F, Jamali-Sheini F, Yousefi R (2015) Photocurrent properties of undoped and Pb-doped SnS nanostructures grown using electrodeposition method. J Electron Mater 44:4734–4739
13. Seal M, Singh N, McFarland EW, Baltrusaitis J (2015) Electro-chemically deposited Sb and in doped tin sulfide (SnS) photo-electrodes. J Phys Chem C 119:6471–6480
14. Hsu HT, Chiang MH, Huang CH, Lin WT, Fu YS, Guo TF (2015) Effects of Ge-and Sb-doping and annealing on the tunable bandgaps of SnS films. Thin Solid Films 584:37–40
15. Patel M, Ray A (2014) Magnetron sputtered Cu doped SnS thin films for improved photoelectrochemical and heterojunction solar cells. RSC Adv 4(74):39343–39350
16. Kumar KS, Manohari AG, Dhanapandian S, Mahalingam T (2014) Physical properties of spray pyrolyzed Ag-doped SnS thin films for optoelectronic applications. Mater Lett 131:167–170
17. Kiruthigaa G, Manoharan C, Bououdina M, Ramalingam S, Raju C (2015) Structural, optical and photocatalytic properties of Ce-doped SnS_2 nanoflakes. Solid State Sci 44:32–38
18. Mariappan R, Mahalingam T, Ponnuswamya V (2011) Preparation and characterization of electrodeposited SnS thin films. Optik 122:2216–2219
19. Sinsermsuksakul P, Chakraborty R, Kim SB, Heald SM, Buonassisi T, Gordon RG (2012) Antimony-doped tin(II) sulfide thin films. Chem Mater 24:4556–4562
20. Liu X, Bai H (2013) Hydrothermal synthesis of visible light active zinc-doped tin disulfide photocatalyst for the reduction of aqueous Cr(VI). Powder Technol 237:610–615
21. Cheng S, Chen Y, Huang C, Chen G (2006) Characterization of SnS films prepared by constant-current electro-deposition. Thin Solid Films 500:96–100
22. Subramanian B, Sanjeeviraja C, Jayachandran M (2001) Cathodic electrodeposition and analysis of SnS films for photoelectro-chemical cells. Mater Chem Phys 71:40–46
23. Ichimuraa M, Takeuchib K, Onob Y, Araib E (2000) Electro-chemical deposition of SnS thin films. Thin Solid Films 361–362:98–101
24. Lee JH, Lee HY, Kim JH, Park YK (2000) Heat treatment of boron-doped CdS films prepared by chemical bath deposition for solar cell applications. Jpn J Appl Phys 39:1669–1674
25. Zainal Z, Hussein MZ, Kassim A, Ghazali A (1997) Electrode-posited SnS thin films from aqueous solution. J Mater Sci Lett 16:1446–1449
26. Nozaki H, Onoda M, Sekita M, Kosuda K, Wada T (2005) Variation of lattice dimensions in epitaxial SnS films on MgO(001). J Solid State Chem 178:245–252
27. Zhao Y, Zhang Z, Dang H, Liu W (2004) Synthesis of tin sulfide nanoparticles by a modified solution dispersion method. Mater Sci Eng, B 113(2):175–178
28. Yue GH, Wang W, Wang LS, Wang X, Yan PX, Chen Y, Peng DL (2009) The effect of anneal temperature on physical properties of SnS films. J Alloys Compd 474(1–2):445–449
29. Kumar KS, Manoharan C, Dhanapandian S, Manohari AG, Mahalingam T (2014) Effect of indium incorporation on properties of SnS thin films prepared by spray pyrolysis. Optik Int J Light Electron Opt 125(15):3996–4000
30. Jamali-Sheini F, Yousefi R, Ali Bakr N, Cheraghizade M, Soo-khakian M, Huang NM (2015) Highly efficient photo-degradation of methyl blue and band gap shift of SnS nanoparticles under different sonication frequencies. Mater Sci Semicond Process 32:172–178
31. Yousefi R, Cheraghizade M, Jamali-Sheini F, Basirun WJ, Huang NM (2014) Effect of hydrogen gas on the growth process of PbS nanorods grown by a CVD method. Curr Appl Phys 14:1031–1035
32. Yue GH, Wang LS, Wang X, Chen YZ, Peng DL (2009) Characterization and optical properties of the single crystalline SnS nanowire arrays. Nanoscale Res Lett 4(4):359–363
33. Reddy NK, Devika M, Hahn YB, Gunasekhar KR (2013) Impact of chemical treatment on the surface, structure, optical and electrical properties of SnS thin films. Appl Surf Sci 268:317–322
34. Cheng S, Hea Y, Chena G (2008) Structure and properties of SnS films prepared by electro-deposition in presence of EDTA. Mater Chem Phys 110:449–453
35. Mathews NR (2012) Electrodeposited tin selenide thin films for photovoltaic applications. Sol Energy 86(4):1010–1016
36. Nair MTS, Mata CL, GomezDaza O, Nair PK (2003) Copper tin sulfide semiconductor thin films produced by heating SnS–CuS layers deposited from chemical bath. Semicond Sci Technol 18:755–759
37. Antunez PD, Torelli DA, Yang F, Rabuffetti FA, Lewis NS, Brutchey RL (2014) Low temperature solution-phase deposition of SnS thin films. Chem Mater 26(19):5444–5446